Propagation of Uncertainty in a Parton Shower*

Philip Stephens† *and André van Hameren*‡
†Kennesaw State University, Department of Physics, 1000 Chastain Road, Kennesaw, GA 30144, USA
‡The H. Niewodniczański Institute of Nuclear Physics, Polish Academy of Sciences, Radzikowskiego 152, 31-342 Kraków, Poland

Abstract
Presented here is a technique of propagating uncertainties through the parton shower by means of an alternate event weight. This technique provides a mechanism to systematically quantify the effect of variations of certain components of the parton shower leading to a novel approach to probing the physics implemented in a parton shower code and understanding its limitations. Further, this approach can be applied to a large class of parton shower algorithms and requires no changes to the underlying implementation.

1 Introduction

As we enter a new era of particle physics, precise knowledge of quantum chromodynamics (QCD) will become increasingly important in order to understand the physics beyond the standard model. Currently, one of the most useful tools for studying QCD is the parton shower approximation. This tool provides a mechanism to connect few-parton states to the real world of high-multiplicity hadronic final states while retaining the enhanced collinear and soft contributions to all orders.

Use of parton shower Monte Carlos (MC) has become common-place. Often, when one needs an estimate of the uncertainty of a MC prediction several different MC programs are used and the differences between them is considered the error [1]. Though this technique of estimating the error of the MC is generally acceptable, it does little to provide insight into the physics. It has been shown [2] that the uncertainties in both the perturbative expansion and the parton distribution functions indeed can lead to effects of the order of ten percent. We propose here a technique in which the known uncertainties of the physics can be propagated through the parton shower framework. This technique provides alternate weights to an event generated by a MC without having to change the basic structure of the MC program. We feel this technique could be valuable when determining how various improvements in the parton shower will impact the MC predictions. Furthermore, this gives a more satisfactory description of the errors in a MC prediction.

*This work is partly supported by the EU grant mTkd-CT-2004-510126 in partnership with the CERN Physics Department and by the Polish Ministry of Scientific Research and Information Technology grant No 620/E-77/6.PRUE/DIE 188/2005-2008.

2 Variation of Parton Shower

In many parton showers [3–6] one starts with the fundamental probability density (for one emission) defined as

$$\mathcal{P} = f_R(\vec{y}) \exp\left(- \int^{\xi(\vec{y})} d^n \vec{y'} f_V(\vec{y'}) \right). \tag{1}$$

Here the function $f_R(\vec{y})$ is the distribution of the real emission while $f_V(\vec{y})$ is the virtual contribution. In both cases the precise definition of $\vec{y}$ is specific to the implementation. Furthermore, the limits of integration in the virtual component are also specific to the implementation: how the infra-red limit is treated, the definition of resolvable versus unresolvable emissions and the ordering of variables. For a time-like shower $f_R = f_V$ and is given by

$$f_R(\vec{y}) = \frac{\alpha_S(g(\vec{y}))}{2\pi} P(\vec{y}), \tag{2}$$

where $g(\vec{y})$ is some abstract function used to determine the scale of the running coupling. We find a similar result for the constrained MC [5]; for a space-like shower using the backward evolution algorithm we find $f_R = f_V f(x, \vec{y})$ and

$$f_V(\vec{y}; x) = \frac{\alpha_S(g(\vec{y}))}{2\pi} \frac{f(x/z, \vec{y})}{f(x, \vec{y})} P(\vec{y}), \tag{3}$$

where $f(x, \vec{y})$ is the PDF at energy fraction x and scale given by some combination of the components of $\vec{y}$. We can explicitly see that one of the components of $\vec{y}$ is z, a momentum fraction.

In the forward (time-like) evolution algorithm, as well as the non-Markovian algorithm, $P(\vec{y})$ is just the Alteralli-Parisi [7] splitting function divided by the scale. In the numerical results here we consider only the forward evolution algorithm; in the last section we propose a use for this technique in a backward evolution algorithm for CCFM.

We now define a functional to represent our functions $f_R(\vec{y})$ and $f_V(\vec{y})$

$$F_R[\boldsymbol{\varphi}(\vec{y})] = f_R(\vec{y}) \,;\, F_V[\boldsymbol{\varphi}(\vec{y})] = f_V(\vec{y}). \tag{4}$$

Here $\boldsymbol{\varphi}(\vec{y})$ are the functional components of $F_{R/V}$ which we want to vary (e.g. the running coupling or the kernel). This defines the distribution of one branching as

$$\mathcal{P}[\boldsymbol{\varphi}(\vec{y})] = F_R[\boldsymbol{\varphi}(\vec{y})] \exp\left(- \int^{\xi(\vec{y})} d^n \vec{y'} F_V[\boldsymbol{\varphi}(\vec{y'})] \right). \tag{5}$$

We can find the variation of this by

$$\delta\mathcal{P} = \mathcal{P}[(\boldsymbol{\varphi} + \delta\boldsymbol{\varphi})(\vec{y})] - \mathcal{P}[\boldsymbol{\varphi}(\vec{y})]. \tag{6}$$

If we define

$$\delta F_{R/V} = F_{R/V}[(\boldsymbol{\varphi} + \delta\boldsymbol{\varphi})(\vec{y})] - F_{R/V}[\boldsymbol{\varphi}(\vec{y})], \tag{7}$$

then

$$\delta\mathcal{P} = \mathcal{P}\left(1 + \frac{\delta F_R}{F_R}\right) \exp\left(- \int^{\xi(\vec{y})} d^n \vec{y'} \delta F_V \right) - \mathcal{P}, \tag{8}$$

from which we have a weight

$$w \equiv \frac{\mathcal{P}+\delta\mathcal{P}}{\mathcal{P}} = \left(1+\frac{\delta F_R}{F_R}\right)\exp\left(-\int^{\xi(\vec{y})} d^n\vec{y}'\delta F_V\right). \tag{9}$$

The weights defined in eqn. (9) are relative to the original probability density for one emission. To get the total weight for the full event, we must consider

$$\mathcal{P}_E[\boldsymbol{\varphi},\{\vec{y}_i\}] = \prod_i \mathcal{P}[\boldsymbol{\varphi}(\vec{y}_i)], \tag{10}$$

and thus

$$\delta\mathcal{P}_E = \mathcal{P}_E[\boldsymbol{\varphi}+\delta\boldsymbol{\varphi},\{\vec{y}_i\}] - \mathcal{P}_E[\boldsymbol{\varphi},\{\vec{y}_i\}]. \tag{11}$$

This leads to a total event weight given by

$$w_E \equiv \frac{\mathcal{P}_E+\delta\mathcal{P}_E}{\mathcal{P}_E} = \prod_i w_i. \tag{12}$$

3 Example Parton Shower Kinematics

For the examples given here we will use as a model bremstrahlung emissions from one quark line. For the numerical results presented in the following sections we use a concrete implementation of the kinematics of the Herwig++ parton shower [3, 8]. In terms of those, we have

$$F_R[\boldsymbol{\varphi}(\vec{y})] = F[(\alpha_S, P_{qq})(z,\tilde{q}^2)] = \frac{1}{2\pi\tilde{q}^2}\alpha_S(z,\tilde{q}^2)P_{qq}(z,\tilde{q}^2)\,, \tag{13}$$

where P_{qq} is the splitting kernel, z is the splitting variable, and $\tilde{q}^2$ is the evolution variable.

4 Kernel Variations

Varying the structure of the splitting kernel may be an interesting example. For example, one could start with the collinear splitting kernels and vary them by the mass dependent quasi-collinear kernels to see whether such changes introduce dramatic effects on a set of observables. The benefit to the procedure presented here is that there is no need to change the fundamental structure of a given MC. In fact one could add an option to their code to keep track of the alternate weights, without changing at all their basic MC program logics and structures. One caveat is that though this method will give an accurate estimate of the variations given, this is only true for regions of phase space in which the original MC fills. If some regions of phase space are empty, or rarely entered, the changes in that region due to the variation will still lack significant statistics.

The collinear kernel is simply

$$P_{qq}(z) = \frac{1+z^2}{1-z}. \tag{14}$$

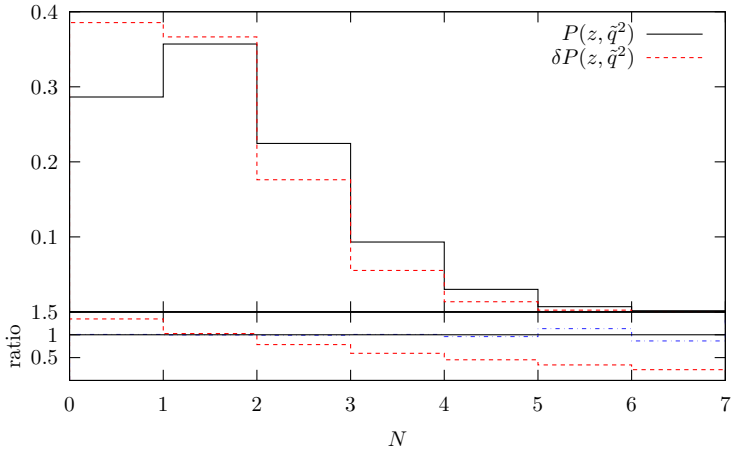

Fig. 1: The distribution of the number of emissions for the collinear kernel and the quasi-collinear kernel for $m^2 = (175\ \mathrm{GeV})^2$ and $\tilde{q}^2 = (1\mathrm{TeV})^2$. The solid line shows the result when the quasi-collinear kernel is used, the dashed line shows the result when the variation in eqn. (15) is applied and the events are weighted. Again, the second panel shows the ratio of the varied to the unvaried MC.

To obtain the quasi-collinear kernel, we must define a variance of

$$\delta P_{qq}(z,\tilde{q}^2) = -\frac{2m^2}{z(1-z)\tilde{q}^2}. \tag{15}$$

With this variance we find the alternate weight, for the ith emission, is given by

$$w_{P_i} = \left(1 + \frac{\delta P_{qq}(z_i,\tilde{q_i}^2)}{P_{qq}(z_i,\tilde{q_i}^2)}\right) \exp\left(-\int_{\tilde{q}_i^2}^{\tilde{q}_{i-1}^2} \frac{d\tilde{q}^2}{\tilde{q}^2} \int_{z_i^-}^{z_i^+} dz\, \alpha_S \left[z^2(1-z)^2\tilde{q}^2\right] \delta P_{qq}(z,\tilde{q}^2)\right), \tag{16}$$

and the total weight due to the kernel variation is the product of the weight for each emission. This weight is normalized to a weight 1 event with no variations.

We now show the result of this variation when showering a top quark with mass $175\ \mathrm{GeV}$ from an initial scale of $1\ \mathrm{Tev}$. In figure 1 we show the effect that the quasi-collinear variation has on the distribution of the number of emissions. As would be expected, for larger masses we have fewer emissions. Figure 2 shows the $p_\perp^2$ spectrum of the outgoing quark. The figures are divided into two panels. The top panel shows the results while the bottom panel shows the ratio of the reweighted MC vs. the unweighted one. In figure 1 the ratio panel also includes the ratio of the reweighted MC vs. an alternate MC sample created by changing the kernel in the MC to the quasi-collinear kernel. We see that this ratio is 1 with small variations.

4.1 Combining Kernel with Running Coupling

Another potential variation that may be of interest is to vary the kernel by a term proportional to the running coupling. Such a variation could be used to introduce some NLO effects into the kernel. If we consider only the lowest order in the variations, then

$$\delta F \approx \delta\alpha_S P_{qq}^{(1)} + \alpha_S \delta P_{qq}^{(1)} + \alpha_S^2 \delta P_{qq}^{(2)}. \tag{17}$$

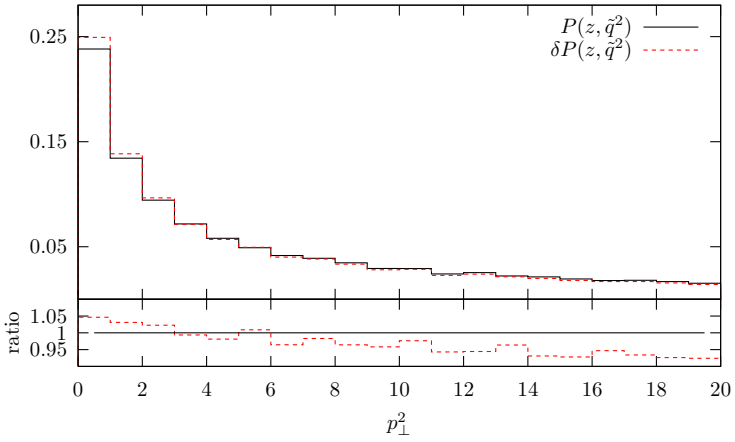

Fig. 2: The distribution of the $p_\perp^2$ of the outgoing quark for the collinear and quasi-collinear cases under the same conditions as figure 1.

We choose the form of $\delta P_{qq}^{(2)}(z)$ according to full NLO kernel [9, 10]. This is composed of two parts, the flavour singlet (S) and non-singlet (V) contributions

$$\delta P_{qq}^{(2)}(z,\tilde{q}^2) = P_{qq}^{S(2)}(z) + P_{qq}^{V(2)}(z), \tag{18}$$

We choose $\delta P^{(1)} = 0$ and $\delta\alpha = 0$ for these examples.

Figure 3 shows the effect on the number of emissions and figure 4 shows the effect on the $p_\perp^2$–spectrum of the outgoing quark line. We see that the number of emissions is slightly higher with a harder spectrum.

The construction of a next-to-leading log (NLL) parton shower has the problem of negative values for the splitting kernels. These destroy the probabilistic interpretation of the Sudakov form factors. Naively, one would assume that this will destroy any meaningful results for the NLL weights. In our case, this is not true. We are reweighting the total density according to the NLL corrections. These may introduce large or negative weights to the reweighted shower, but this is necessary as this correctly describes the density. In the inclusive picture, these negative weights are integrated over and pose no problem; exclusively, these negative weights must be treated correctly in the analysis.

5 Variation of Kinematics

We now consider another use of the alternate weights. Here we wish to use these weights to transform one parton shower into another. This, of course, is not an exact transformation. This requires additional knowledge about the structure of the alternate parton shower.

The idea is to use the variables generated by one shower and reshape the distribution to give the results if an alternate shower was used. In this section we discuss the intrinsic kinematical definitions.

Consider a new kinematics, similar to the one used in Pythia [4]. Here we wish to order the parton shower in virtuality (Q^2). This requires a mapping from $\tilde{q}^2$ into Q^2. Furthermore,

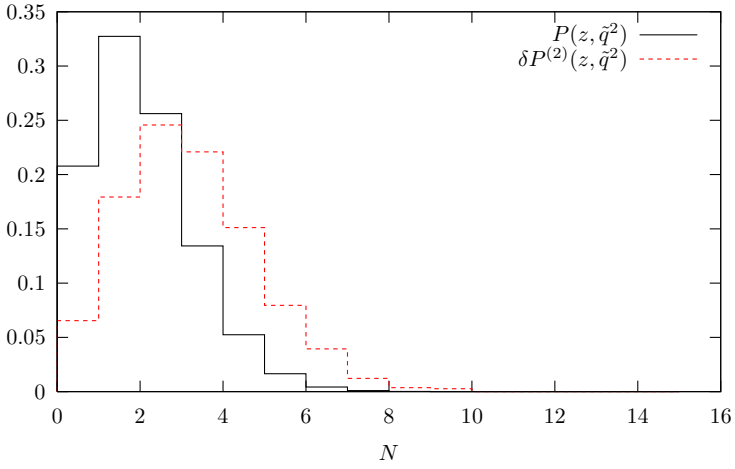

Fig. 3: The distribution of the number of emissions using the collinear kernel at $\mathcal{O}(\alpha_S)$ and applying the variation discusses in the text at $\mathcal{O}(\alpha_S^2)$.

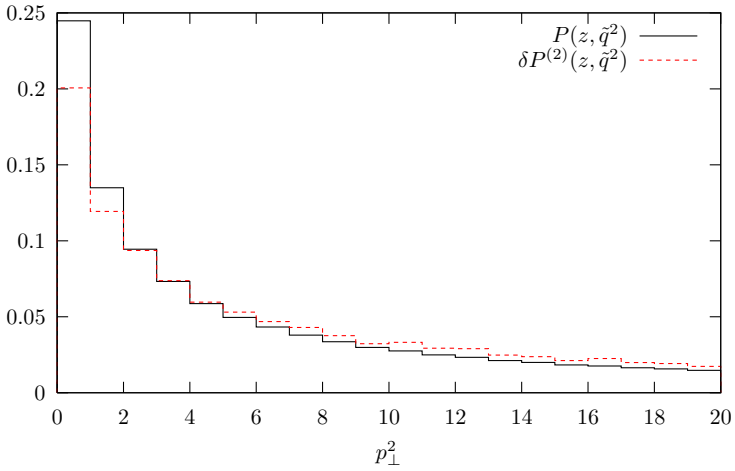

Fig. 4: The $p_\perp^2$ distribution of the outgoing quark under the same conditions as figure 3.

there is a different interpretation of the meaning of the momentum fraction z in the Pythia-like and Herwig-like shower; they have the same distribution, however. We compensate for this by constructing the full four-momentum from the Herwig-like shower and deconstructing the associated variables for each emission. The weights can then be computed from this. This method has the additional benefit that the four momentum configuration is identical in both cases; thus hadronization effects and hadron decays are identical. We define our variations such that

$$\bar{F}[(\alpha_S, P_{qq})(\bar{z}, Q^2)] = F[(\alpha_S, P_{qq})(z, \tilde{q}^2)] + \delta F, \tag{19}$$

where the left-hand side refers to the Pythia-like shower. From this we find

$$\delta F = \bar{F}[(\alpha_S, P_{qq})(\mathcal{T}(z, \tilde{q}^2))]\mathcal{J}(\bar{z}, Q^2) - F[(\alpha_S, P_{qq})(z, \tilde{q}^2)], \tag{20}$$

where $\mathcal{J}$ is the Jacobian factor for the coordinate transformation $\mathcal{T}(z, \tilde{q}^2)$ from the Herwig-variables to the Pythia variables. At this point we can exploit the analytic structure of the Sudakov form factor,

$$\Delta(t; t_0) = \Delta(t; t_1)\Delta(t_1; t_0). \tag{21}$$

This allows the seperation of the weights into the real and the Sudakov components and to calculate the Sudakov components over the full evolution scale, rather than just the scales between each emission. This gives

$$w_\Delta = \frac{\Delta_P(Q^2_{ini}; Q^2_0)}{\Delta_H(\tilde{q}^2_{ini}, \tilde{q}^2_0)}. \tag{22}$$

The total weight is given simply as

$$w = w_\Delta \prod_{i=1}^{N} w_i^{(R)}, \tag{23}$$

where the $w_i^{(R)}$ refer to the weights for the real emissions.

The question now is what does the weighted shower physically give us? This gives us the weight, relative to the unweighted original shower, of producing the kinematical configuration via the other shower. For our example here this means that it will weight our Herwig-like shower to be that of the Pythia-like construction. Our weighted shower will produce events that are both ordered in virtuality and in angle. Comparing the weighted results versus an independent implementation of the full Pythia-like shower would illustrate, for any observable ,the effect of the different limits in phase-space inherent in each implementation. Furthermore, it could be used to illustrate the effects of alternate choices of ordering; e.g. colour connections between jets.

To illustrate this technique we use as a model $e + e-$ annihilation into a $q\bar{q}$ pair. This pair then undergoes final state radiation, but the subsequent emissions do not. We reconstruct the kinematics of the event and, in order to conserve $\sqrt{s}$, we rescale each jet by a common factor, k, such that

$$\sqrt{s} = \sum_{i=1}^{N} \sqrt{q_i^2 + k\boldsymbol{p}_i^2}, \tag{24}$$

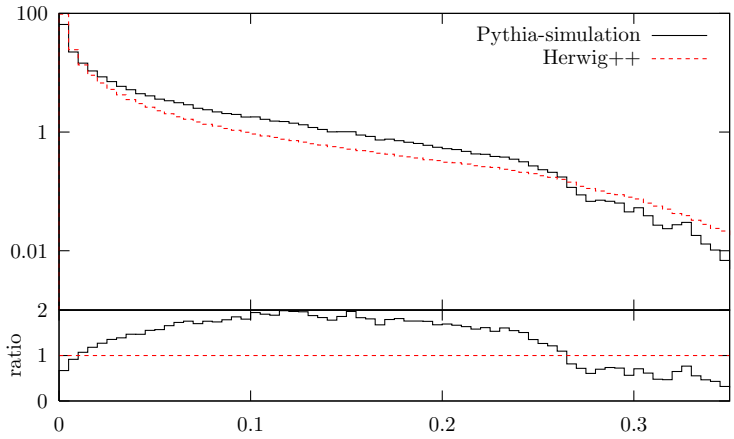

Fig. 5: $1 - T$ for the Herwig-like shower and reweighted to a Pythia-like shower, as described in the text. These differences are due to the different kinematics definitions used in each shower. The bottom panel shows the ratio of the Pythia-like vs. Herwig-like.

where q_i^2 is the virtuality of jet i. To illustrate the reweighting between the Herwig-like and Pythia-like shower we study the thrust observable. This is given by

$$T = \max_{\boldsymbol{n}} \frac{\sum_{i=1}^{N} |\boldsymbol{p}_i \cdot \boldsymbol{n}|}{\sum_{i=1}^{N} |\boldsymbol{p}_i|}. \tag{25}$$

This observable was chosen as the thrust has a strong correlation to the hardest emission, but also is effected by subsequent emissions. As we don't shower the emitted gluons, studying an observable which have a strong dependence on 2 or more emissions is not as illustrative.

Figure 5 shows the result for $\sqrt{s} = 1$ TeV. We can see the deviations, and as expected they are not too large. As these are not the result of a full event generation it is not useful to compare these to data.

6 Uncertainty in Unintegrated Parton Distribution Functions

In the last example we show how to apply the technique to compute the effect of uncertainties in the unintegrated parton distribution function (updf) for the backwards evolution algorithm of CASCADE [11]. In this algorithm the updfs are taken from the outputs of an alternate Monte Carlo algorithm, based on SMALLX [11–13]. This leads to large uncertainties in the updfs. Additionally, in order to fit the initial conditions of the updf MC, based on SMALLX, one must match the output of CASCADE to data. The ability to take the uncertainty of the updf MC into account will allow for better fits overall. Figure 6 shows a schematic of this procedure.

We present here the formula needed to compute the effect of the updf uncertainties in the CASCADE algorithm. We do not endeavor here to implement these weights in the CASCADE program, nor suggest the ideal treatment of this information. This is left as future exercises for the authors of CASCADE.

The CCFM equation describes the gluonic structure of the proton. The variables of this

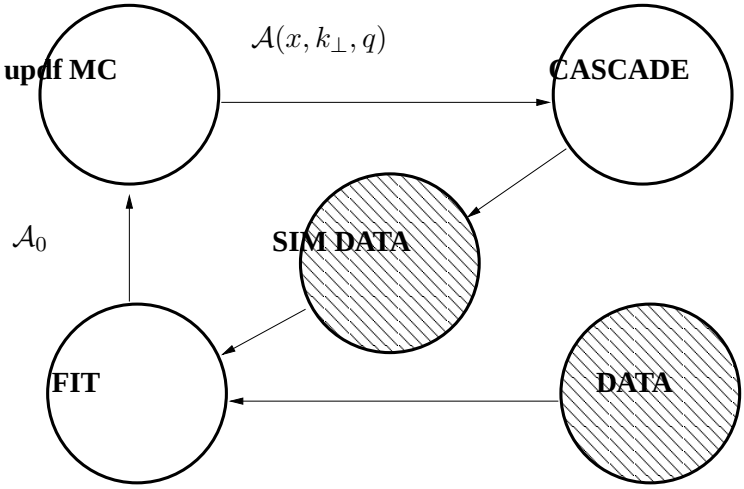

Fig. 6: Schematic of the flow of the fitting procedure using CASCADE and updf MC. As the output of the updf MC is not directly fitted, rather that of CASCADE, tracking uncertainties from the updf MC through CASCADE can prove useful in the fits.

evolution are a scale, q, the momentum fraction, x, and the transverse components, $k_\perp$. In CASCADE, given a step in the evolution terminates at q, x and $k_\perp$, the probability of evolving to a new $\bar{q}, x/z$ and $k'_\perp = |(1-z)/z\boldsymbol{q} + \boldsymbol{k}_\perp|$ is

$$\begin{aligned}\mathcal{P}(\bar{q}, z, \phi, k'_\perp; q, x, k_\perp) &= \frac{\tilde{P}(z, \bar{q}/z, k_\perp)}{2\pi z q^2}\mathcal{A}(x/z, k'_\perp, \bar{q}/z) \\ &\times \exp\left(-\int_q^{\bar{q}} \frac{dq'^2}{q'^2}\int \frac{dz}{z}\frac{d\phi}{2\pi}\tilde{P}(z, q'/z, k_\perp)\frac{\mathcal{A}(x/z, k'_\perp, q'/z)}{\mathcal{A}(x, k_\perp, q')}\right),\end{aligned} \tag{26}$$

where $\tilde{P}$ is the kernel including the non-sudakov form factor and $\mathcal{A}$ is the updf. In contrast to the previous examples, here the real and virtual contributions are clearly different. When we propogate the variance of the updf in the real function we find

$$\frac{\delta F_R[\boldsymbol{\varphi}]}{F_R[\boldsymbol{\varphi}]} = \frac{\delta\mathcal{A}(x/z, k'_\perp, q'/z)}{\mathcal{A}(x/z, k'_\perp, q'/z)}. \tag{27}$$

In the virtual case this is more complex. Here we find

$$\delta F_V[\boldsymbol{\varphi}] = \frac{\tilde{P}(z, q'/z, k_\perp)}{2\pi z q'^2}\left(\frac{B+\delta B}{A+\delta A} - \frac{B}{A}\right) \approx \frac{\tilde{P}(z, q'/z, k_\perp)}{2\pi z q'^2}\frac{1}{A}\left(\delta B - B\frac{\delta A}{A}\right), \tag{28}$$

where

$$A \equiv \mathcal{A}(x, k_\perp, q')\ ;\ B \equiv \mathcal{A}(x/z, k'_\perp, q'/z). \tag{29}$$

These formulae can be used to give the weight associated with the uncertainty due to the updf. Of course, implementation of this weight in the CASCADE framework requires still some work. Once complete, however, use of this alternate weight during the fitting procedure should help improve overall predictions of the model.

7 Conclusion

We have presented a new approach to understanding the errors associated with a MC prediction. This approach can be added to almost all currently existing MC programs without changing the physics or the behaviour of the code. Instead, we have provided a method to track alternate weights for events. These alternate weights provide the tool to reshape MC predictions to see what such a prediction would be if various pieces of the MC were altered.

Though this technique is quite successful, it cannot compensate for all possible alterations. As this algorithm provides an alternate weight for an event generated by a MC it cannot provide events which cannot be generated by the original MC. This means that some of the physical limitations of an already existing code cannot be overcome through this method. We don't see this as a drawback, however. The purpose of this technique is to understand the physics and the limitations inherent in a MC implementation. To this end, such limitations of this technique can provide valuable insight.

This paper has provided numerical examples of a toy parton shower model based on the real MC behaviour of Herwig++ [3, 8]. It may be quite illustrative to apply this method to a fully featured general purpose MC, including hadronization and hadron decay, to see how much variation exsists in such a parton shower implementation. With such an implementation one may be able to check the accuracy of many MC predictions and to understand the limitations of these predictions.

Acknowledgment

The authors would like to thank S. Jadach and Z. Wąs for many useful discussions.
Additionally, PS would like to thank H. Jung for suggesting the use of this method for the CASCADE fitting procedure.

References

[1] Grunewald, Martin W. and others (2000).

[2] Gieseke, Stefan, JHEP **01**, 058 (2005).

[3] Gieseke, S. and Ribon, A. and Seymour, M. H. and Stephens, P. and Webber, B., JHEP **02**, 005 (2004).

[4] Sjostrand, Torbjorn and others, Comput. Phys. Commun. **135**, 238 (2001).

[5] Jadach, S. and Skrzypek, M., Comput. Phys. Commun. **175**, 511 (2006).

[6] Gleisberg, Tanju and others, JHEP **02**, 056 (2004).

[7] Altarelli, G. and Parisi, G., Nucl. Phys. **B126**, 298 (1977).

[8] Gieseke, S. and Stephens, P. and Webber, B., JHEP **12**, 045 (2003).

[9] Furmanski, W. and Petronzio, R., Phys. Lett. **B97**, 437 (1980).

[10] Curci, G. and Furmanski, W. and Petronzio, R., Nucl. Phys. **B175**, 27 (1980).

[11] Jung, H. and Salam, G. P., Eur. Phys. J. **C19**, 351 (2001).

[12] Marchesini, G. and Webber, B. R., Nucl. Phys. **B386**, 215 (1992).

[13] Marchesini, G. and others, Comput. Phys. Commun. **67**, 465 (1992).